Techniques for Schumann Resonance Measurements: A Comparison of Four Amplifiers With a Noise Floor Estimate

José A. Gázquez Parra, *Senior Member, IEEE*, Manuel Fernández Ros, Nuria Novas Castellano, and Rosa M. García Salvador

***Abstract*— Schumann resonances are very weak natural electromagnetic signals produced in the earth–ionosphere cavity located in the extremely low frequency (ELF) band (7–60 Hz), and the sensors that measure them produce amplitudes of few microvolts. Strong signals from power lines (50–60 Hz) occur in the same frequency range. Amplification techniques play a key role in acquiring resonance modes with the best signal-to-noise (S/N) ratio. This paper presents a study of the various structures of amplification systems that optimize the S/N ratio for the signal of interest. The aim of this paper is to measure all possible resonance modes with low time acquisition. To this end, we compare four instrumentation amplifiers and design a new indirect method for obtaining the noise floor of the system with sensors manufactured on magnetic cores that are several meters long. We present the measurements of the Schumann resonance achieved using these techniques at the ELF electromagnetic wave observatory at Calar Alto (Spain). The solutions adopted allow measurement of seven resonance modes with an acquisition time of 30 min, where the S/N ratio in the fundamental mode was 39 dB.**

***Index Terms*— Extremely low frequency (ELF) band, instrumentation amplifier (IA), magnetic sensor, measurement, noise, Schumann resonance.**

I. Introduction

THE electromagnetic waves due to natural phenomena and human activity that reach the earth's surface cover a wide range of frequencies in the spectrum. In the extremely low frequency (ELF) range, the 5–100 Hz band is associated with a phenomenon known as the Schumann resonance [1]. This phenomenon occurs in the cavity formed by the earth's surface and the ionosphere, which acts as a waveguide for ELF signals arising from electrical activity in the atmosphere [2]. Measurement of this phenomenon allows characterization and diagnosis of the terrestrial environment [3] as well as the calibration of global temperature [4]. It can also be considered a tool for preventing earthquake disasters [5] and for measuring lightning activity [6] and the average conductivity of the earth's ionosphere [7]. This natural phenomenon can also be applied to investigate the electromagnetic environment of other planets in the solar system and to provide information on climate and other properties of the lower part of any planet that has an ionosphere [8].

The majority of published papers are related to the study of ELF wave propagation in the earth–ionosphere cavity, demonstrating the complexity of the measurement process and amongst other factors, the nonuniformity of the ionosphere, the presence of natural electromagnetic noise [9], the presence of interference in industrial areas, and background noise [10]. Studies tend to present the spectral characteristics of the resonance models and their amplitude [11], making comparisons between observed data and theoretical models of components for the magnetic field associated with the phenomenon [12] as well as variations in the signals, depending on local and universal time [13].

These studies consider only the first three resonance modes, located in the frequency range 7–28 Hz [14]. Occasionally, capture extends to the fourth mode [15] although, under extreme conditions of nearby lightning strikes, up to 13 modes have been observed [16].

Very few publications give any indication of the general aspects of the measurement system used, given that they should be comprised of a receiving magnetic loop antenna, low-noise amplifier, low-pass filter, an A/D converter, and a datalogger [17]. A recent publication [18] presented descriptively a measuring station of Schumann resonances in Mexico, but no details of measurement electronics are given. In no instance do the authors consider problems such as those arising from the electrical characteristics of the sensor, its adaptation to the amplification system, the structure and analysis of the amplification system, or the low-level signal obtained. In addition, they do not provide data regarding the noise where the signal is embedded, the signal-to-noise (S/N)

Manuscript received November 14, 2014; revised March 2, 2015; accepted March 3, 2015. Date of publication June 15, 2015; date of current version September 11, 2015. This work was supported in part by the Ministry of Economic and Competitiveness of Spain, under Project TEC201460132P, in part by the European Union FEDER Program, and in part by Innovation, Science and Enterprise, Andalusian Regional Government through the Electronics, Communications and Telemedicine TIC019 Research Group of the University of Almeria, Almería, Spain. The Associate Editor coordinating the review process was Dr. Subhas Mukhopadhyay.

J. A. G. Parra, N. N. Castellano, and R. M. G. Salvador are with the Department of Engineering, University of Almeria, Almería 04120, Spain (e-mail: jgazquez@ual.es; nnovas@ual.es; rgs768@ual.es).

M. F. Ros is with the Consejería de Educación, Cultura y Deporte, Andalusian Regional Government.

Color versions of one or more of the figures in this paper are available online at http://ieeexplore.ieee.org.

Digital Object Identifier 10.1109/TIM.2015.2420376

ratio of the measured signal or the method for obtaining it. Moreover, several hours or days are usually needed to provide relevant data from the ELF signals [11] without regard to the benefits to be achieved by reducing the averaging time because long records of resonances can vary over the acquisition time, leading to an incorrect assessment of the results. The need to reduce the noise in spectral estimation techniques is a topic of current interest [19]. A solution would be to reduce the amplifier noise to a possible minimum. Levinzon [20] and Roshan-Zamir and Ashtiani [21] proposed methods of reducing noise through an amplifier by using a field effect transistor (FET) preamplifier. Other recent studies are focused on noise reduction in amplifiers coupled by capacitor [22]. But an evaluation of the S/N ratio is indispensable for obtaining quantitative rather than qualitative assessments of ELF signals. Optimization of the amplification system will enable an improvement of the S/N ratio and a reduction in the capture time needed for their analysis in the frequency domain.

To study the ELF electromagnetic waves, the University of Almeria designed the first observatory of ELF waves in Spain at Calar Alto (Almeria province) and began operation in 2011. The observatory consists of two magnetic antennas, oriented north–south and east–west. Each antenna consists of two symmetrical windings, providing balanced differential signals to minimize common mode effects [23].

The offline study undertaken at the Universidad de Almería estimated the spectral density based on fast Fourier transform algorithms using averaged periodograms [24].

A complex study for measuring the Schumann resonances is required to correctly quantify the measurements and optimize the time averaging. By developing these systems, the efficiency of capture of the signals coming from the Schumann resonance will be improved, thereby facilitating their subsequent study and analysis.

The present study has the following objectives.

1) Design an optimal amplification system for measuring ELF signals and, in particular, the Schumann resonances. This system must meet certain specifications, such as low noise, minimal intermodulation, filtering of power line signals, and it must use techniques that improve the overall dynamic range of the system.
2) Perform a comparison from a noise perspective using four instrumentation amplifiers (IAs) supplied by three leading manufacturers.
3) Design a new method for obtaining the noise floor of the system, which allows an assessment of the S/N ratio of the signals obtained and sensors manufactured on magnetic cores that are several meters long.

II. ELF Sensors and Intrinsic Noise

The structure of the measurement system needs to consider the characteristics of the sensors that comprise it because these elements act as the source of the signal for the system. Because of the frequency range to be measured, the sensors usually used are coils with a magnetic core and a large number of windings with high internal impedance that is dependent on the operating frequency. Fig. 1 shows the classic model of a sensor coil and its series equivalent circuit.

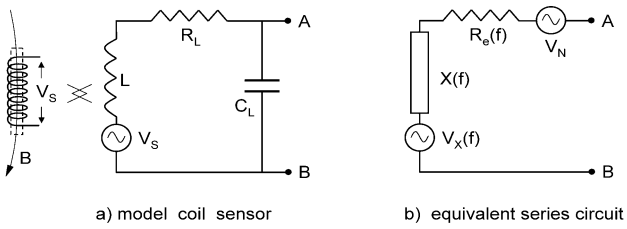

Fig. 1. Model of a sensor coil.

TABLE I
Sensor Characteristic

Sensor	Φ (mm)	n	l_{core} (m)	R_L(kΩ)	L(H)
Sensor 1	0.5	29225+29225	2	1.35	479
Sensor 2	0.5	29225+29225	2	1.35	943
Sensor 3	0.15	150000+150000	2	34	11632

As it crosses a solenoid L, the magnetic field B induces an electrical voltage V_S in accordance with Faraday's law (1), where A is the surface area of the solenoid and n is the number of windings

$$V_S(t) = A \cdot n \cdot \frac{dB}{dt}. \tag{1}$$

In the case of sinusoidal signals: $B(t) = \overline{B} \cdot \sin(\omega t)$, the induced voltage is expressed by

$$\overline{V}_S(\omega) = A \cdot n \cdot \omega \cdot \overline{B}. \tag{2}$$

Because of the dependence of the induced signal on factor $\omega \cdot \overline{B}$, a cored coil with a large number of turns in the ELF range cannot be modeled; thus, no formal relationship can be obtained between the voltage induced by the magnetic field, V_s [from Fig. 1(a)], and the voltage of the generator $V_X(f)$ of the series equivalent circuit of the sensor [Fig. 1(b)]. To establish this relationship, we have to study the response of a source-sensor-amplifier system, as described in Section III. The correct characterization of the sensor in terms of adaptation and noise requires the experimental measurement of the impedance versus frequency $Z(f)$ to determine the adaptation characteristics and the spectral density of the noise. The noise can be modeled in the series equivalent circuit using a generator $V_N(f_i)$, which is a function of the real part of the impedance $\mathrm{Re}[Z(f)]$ and the frequency

$$V_N(f_i) = \sqrt{4KT\ \mathrm{Re}[Z(f_i)]} \tag{3}$$

where K represents the Boltzmann constant and T is the temperature in kelvin degrees. Trials were established using three balanced sensors and a high-permeability core. Table I shows the most important characteristics: Φ is the diameter of the thread, n is the number of windings, l_{core} is the length of the core, R_L is the resistance of the sensor in dc, and L is the inductance at 5 Hz, considering a single section of the balanced coil.

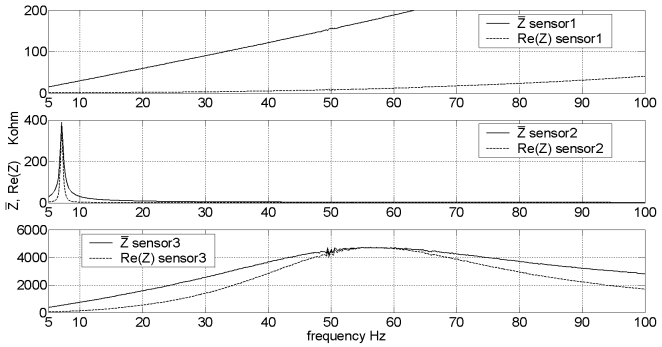

Fig. 2. Comparison of sensors in terms of the Z module and its real part Re(Z).

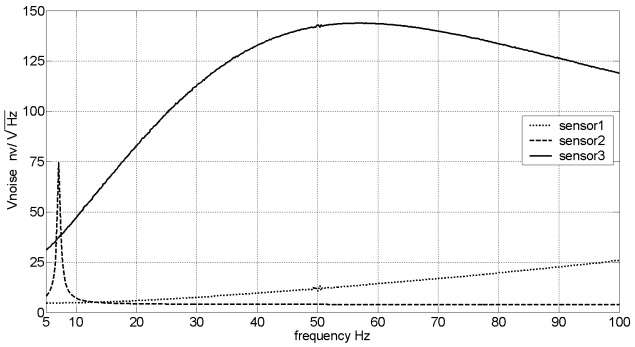

Fig. 3. Spectral density of noise for sensors connected at 5 MΩ.

The difference between sensors 1 and 2 is their self-resonance: in sensor 1, self-resonance is far away from 0 to 100 Hz range, and this enables measurements of up to 1 KHz. Moreover, sensor 2 is resonant at 7.5 Hz and is only suitable for high-resolution measurements of the first Schumann resonance mode. Sensor 3 was designed, so that it has a bandwidth of 0–100 Hz.

A. Characterization of the Sensor

Characterization of the ELF sensors was performed using a vector network analyzer (VNA), model E5061B (Agilent). The most direct method for measuring an impedance Z using a VNA is by measuring the S_{11} port, which provides a direct ratio with Z. Using this method, the higher the impedance, the larger the error, because Z is measured in relation to the characteristic impedance Z_o. For values of impedance of hundreds of kiloohms, the error invalidates the measurement. Another method consists of using the impedance Z as a quadrupole between the two ports of the VNA and measuring the transmission parameter S_{21} [25]. This parameter is given in (4) from which the impedance Z is obtained by means of (5)

$$S_{21} = \frac{2Z_0}{Z + 2Z_0} \tag{4}$$

$$Z = 2Z_0 \left(\frac{1}{S_{21}} - 1 \right). \tag{5}$$

This method was used for values of Z greater than 5 MΩ. It has very little error in the low-frequency range and is considered adequate for characterizing sensors that have a large number of fine windings, such as sensor 3.

The real part of the sensors impedance depends on the frequency. Fig. 2 compares the impedance module of each sensor (Z) and the real part of this impedance (Re(Z)). One can see that in sensor 3, there is close coincidence between Z and Re(Z); likewise, in sensor 2 even though here, the coincidence is not as close. In contrast, the divergence in sensor 1 spans an order of magnitude.

Based on the experimental impedance curves of the sensor, we can represent $V_N(f_i)$ and calculate the total noise that it introduces into the measurement frequency range.

Fig. 3 compares the spectral density of thermal noise from the sensors connected to an amplifier with an input impedance of 5 MΩ. We can see that in sensor 3 (with its large number of turns of fine wire) there is greater thermal noise than in the other sensors, which have a shorter length of thicker copper wire.

The total noise V_{NT} is calculated numerically for a particular temperature, given that the vectors for the real part of the impedance Re[Z(f)] increase as the frequency increases

$$V_{\mathrm{NT}} = \sum_{f=f_1}^{f_2} \sqrt{4KT\ \mathrm{Re}[Z(f)] \cdot \Delta f} \tag{6}$$

where f_1 and f_2 are the lower and upper frequencies of the range, in which the total noise of the sensor is determined, and Δf is the frequency increment of vector Re[$Z(f)$]. Knowing the total noise of the sensor, we can determine the equivalent noise resistance R_{Neq} (7). This parameter is useful for comparing the noise of the sensor with the noise of the amplifier within the frequency range being studied, $B = f_2 - f_1$

$$R_{\mathrm{Neq}} = \frac{V_{\mathrm{NT}}^2}{4KTB} \tag{7}$$

where K represents the Boltzmann constant and T is the temperature.

The total noise obtained at 300 K in sensor 1 was 0.20 μV. In sensor 2, it was 0.11 μV and in sensor 3, it was 2.5 μV. The noise in sensor 3 is an order of magnitude higher than the others, even though this factor does not determine the efficiency of the measurements because the sensor may deliver a greater signal level than the others. To determine the quality of the measurements, it is necessary to compare the signal measured against the total noise of the system.

III. Amplification System

The amplification system is heavily dependent on the input impedance, sensitivity, and noise because of the characteristics of the sensor, which will determine its structure and gain.

A. Impedance Matching of the Sensor Amplifier

With respect to the adaptation of the sensor amplifier, it is very important to study the impedance of the sensors as a function of frequency. The loading effect on the sensor amplifier and the noise generated in the system are conditioned

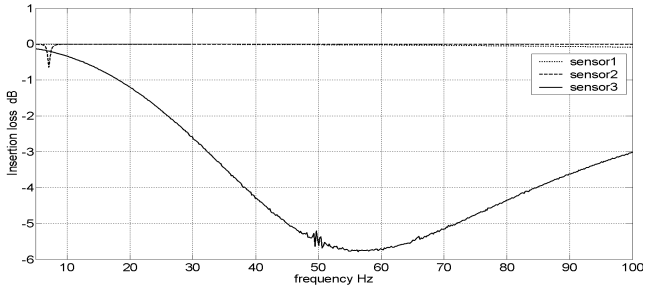

Fig. 4. Insertion losses of the sensors with $Z_i = 5$ MΩ.

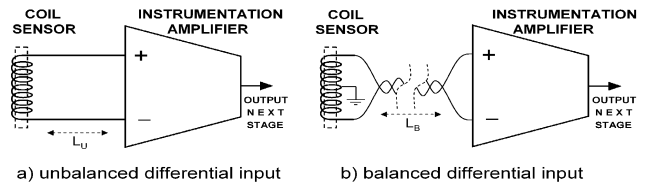

Fig. 5. Connection between the sensor and first-stage amplifier.

by the dependence of the real part of the sensor's impedance on frequency. Therefore, the value of the direct current resistance of the sensor is not a valid value (Fig. 2).

On the basis of the impedance data from the sensors studied, the need for a first amplifier stage with high-input impedance and low noise is confirmed, and an IA is the most suitable for this stage.

According to the data in Fig. 2, the dominant part of the impedance is the real part, and it is not appropriate to establish a passive network that fits the imaginary part because the detriment in the nonlinear response does not compensate for the improvement in insertion.

To determine the insertion losses for each case, we need to numerically solve for the attenuation value as a function of the frequency. Fig. 4 shows the insertion losses of the three sensors with respect to frequency, connected to an amplifier with a 5 MΩ input resistance. This value might be considered high, but note that the standard oscilloscopes have an input resistance of 1 MΩ, and 10 MΩ with a ×10 attenuator probe.

Sensor 3 exhibits the greatest insertion losses and is greater than 5 dB at certain frequencies, while sensors 1 and 2 do not show any appreciable losses. In view of the above results, it is clearly important that the input impedance of the first amplifier stage has a value high enough to avoid the loss of a large proportion of the energy delivered by the sensor when connecting to the amplifier.

B. Sensor-Amplifier Transmission Line

The connection of the sensor to the amplification system will always be in differential mode. Nondifferential connections imply a significant degradation of the signal due to the capture of common mode signals because the cable acts as an electrical antenna. For the differential connections, the unbalanced configuration [Fig. 5(a)] has the drawback of the sensor-amplifier connection cable capturing unwanted signals, thus constraining its length. This problem is typical

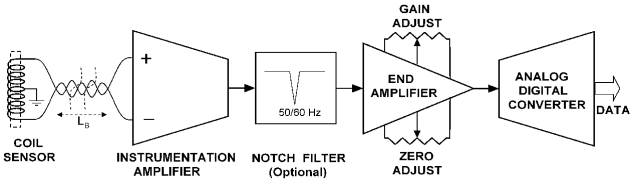

Fig. 6. Structure of the measurement system.

for cases of stage adaptation for audio [26], whereas selecting balanced configurations [Fig. 5(b)] allows a cable length of 10 m without attracting unwanted signals. In field trials, we discovered the benefit of using a balanced configuration, which allowed a cable length of 10 m without increasing the level of interference from the main supply. The sensor was grounded using a copper peg because without this, we captured signals generated by instruments used during the setup of the installation, such as portable oscilloscopes. The electrical effect of the cable can be modeled by only considering the value of the distributed capacitor C_C presented by a cable, in parallel with the sensor output with a value proportional to the length of the cable in which case, the use of cables with low distributed capacitance (<100 pF/m) is advisable. The distributed effects in transmission lines in the ELF band are negligible for lengths of a few tens of meters. Fig. 5 shows different connection configurations.

C. Amplification Stage

The most suitable structure for the first-stage amplification, with a specification for a high-input impedance ($Z > 1$ MΩ) and high gain ($G > 60$ dB) corresponds to an IA.

The tests undertaken lead us to believe that the system will require a gain of between 60 and 110 dB. The first stage can provide a gain of up to 60 dB without instability problems. To achieve the remaining gain, a second amplification/conditioning stage is required and does not demand a high-quality IA, so that two low-noise, high-precision operational amplifiers (OAs) are sufficient. Fig. 6 shows the overall structure of the system.

The measurement system includes an optional notch filter implemented using an active cell in double T [27] to attenuate the signal from the main supply (Fig. 6). The filter is inserted between the two amplification stages to prevent the degradation of the overall noise figure, even though this filter is optional. This type of filter is useful when taking measurements close to power lines or when the high intensity of signals from the power lines, captured by the sensor, saturate the dynamic range to produce minimal gain because it has a negative effect on the linearity of the data and poses problems around the suppressed frequency.

During the development of this system, four IAs were tested. The models tested were AD524 [28], INA110 [29], INA126 [30], and LT1167 [31]. These models are, currently, the most relevant devices of different brands, and they range from very low-cost amplifiers (INA126) to the most expensive amplifiers, including top of the range (AD524). Amplifiers AD524 and INA110 feature an integrated resistance setting that can access preset gains without the need for

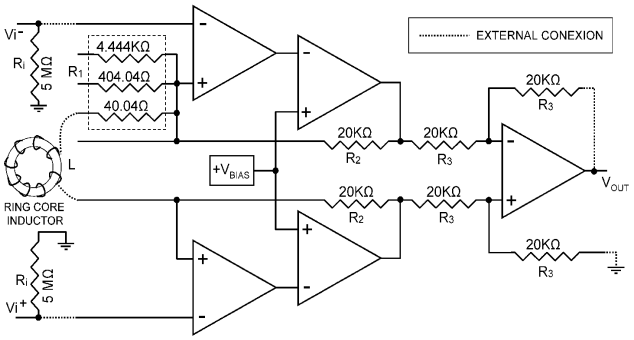

Fig. 7. Structure of the IA, AD524.

external components. Fig. 7 is a scheme of the internal make-up of amplifier AD524. In addition, the noise sources of these resistances can be included; these sources are among the features provided by the manufacturers. The LT1167 and INA126 models are IAs that require additional external resistances to fix their gain. The internal configurations of amplifiers INA110, INA126, and LT1167 are traditional with three OAs, while amplifier AD524 is configured with five OAs, which means it has a broader bandwidth (Fig. 7).

For amplifiers AD524 and INA110, the maximum gain possible was selected for their internal resistances, 60 and 54 dB, respectively. For amplifier LT1167, a gain of 60 dB was selected and for amplifier INA126, a gain of 54 dB was selected. We limited the gain of these amplifiers to 60 dB because of the instability problems encountered during the tests. The high gain used for each of the devices together with the high impedance of the sensors led to the use of input resistances of 5 MΩ for all of the amplifiers, and the AD524 amplifier was the one with the greatest tendency for instability as the resistance seen by the inputs increased.

The selection of these high gain values causes the band of the amplifier to be limited, but it is not possible to use capacitors because of the lack of access to the internal resistances in models AD524 and INA110. One solution to resolve the band limitation is to introduce an inductor in series with R_1 (Fig. 7). According to (8), a pole is introduced at $S = S_1$. In the circuit, L has a value of 60 mH, which situates the pole at approximately 100 Hz. The inductor is made of a material called T38 around a ring core, which means it has a small size, few windings, and an insignificant internal resistance in comparison to R_1. In addition, the ring core minimizes the capture of the external field

$$G_V = 1 + \frac{2\frac{R_2}{R_1}}{1 + \frac{L}{R_1}S} \rightarrow \quad S_1 = -\frac{R_1}{L}. \tag{8}$$

The final amplifier stage was realized using the LM833 subsystem, which consists of two, low-noise OAs joined in cascade, sharing the gain between the two substages such that the total gain of the system can be adjusted between 0 and 52 dB. Fig. 8 shows the final amplifier diagram that delivers the signal to the A/D converter.

Amplifier U_1 has an adjustable gain from 1 to 40, and its values are given in Table II. The capacitor array (C_1 to C_8) allows two poles to be maintained at 100 Hz for any of the gains selected.

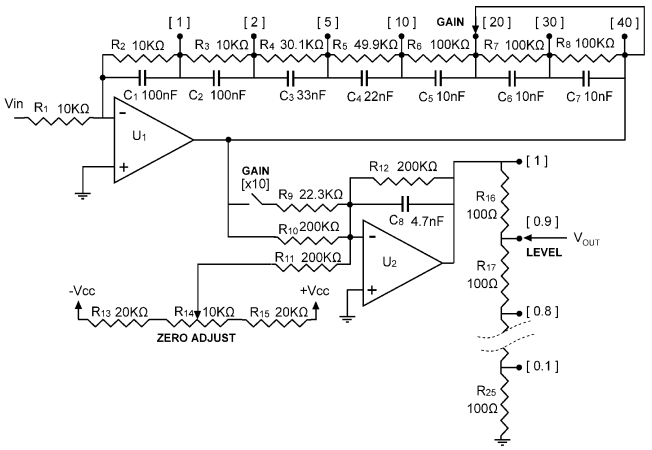

Fig. 8. Diagram of the final amplifier.

TABLE II
GAIN OF AMPLIFIER U_1 IN THE FINAL STAGE

Gain	1	25	10	20	30	40
G(dB)	0	614	20	26	29.5	32

TABLE III
REDUCTION IN OUTPUT LEVEL

Reduction	1	0.9	0.8	0.7	0.6	0.5	0.4	0.3	0.2	0.1
dB	0	-0.9	-2	-3	-4.5	-6	-8	-10.5	-14	-20

Amplifier U_2 has a summing configuration to correct the zero adjustment before delivering the signal to the conversion stage. With the switch GAIN[$\times$10], we can set the gain to 0 or 20 dB. Moreover, the resistance array (R_{16} to R_{25}) of the output is configured as a volume selector that reduces the overall gain of the system. This adjustment is required so that no clipping occurs in the input stages of the A/D converter because the converter used has a narrower dynamic range than the dynamic range of the amplifier. Table III shows the reduction factors of the output level.

The resistances R_{13} (10 kΩ), R_{14} (20 kΩ), and R_{15} (20 kΩ) are used for the zero adjustment, given that the A/D converter introduces a certain direct component at its input.

D. Noise Study

With the test amplifiers, we proceeded to the theoretical calculation of the equivalent input noise RTI using the method provided in [32]. Then, we tested it with resistors of different input values, simulating the internal impedances of possible signal sources. The resistor values tested were 0 (short circuit), 1.2, 25, 110, 220, and 470 kΩ. The goal was to determine the rms noise and spectral distribution of the equivalent input noise referred to the input (RTI) by comparing their behavior to different signal sources characterized by their internal impedance.

Table IV gives a summary of the data for calculating noise taken from the manufacturers' datasheets. The following

TABLE IV
FEATURES OF THE IAs

	AD524	INA110	LT1167	INA126
Noise voltage (nV/√Hz)	7	10	7.5	35
Flicker voltage (1Hz) (nV/√Hz)	10	100	25	200
Corner frequency (Hz)	2.5	600	7	30
Noise Current (fA/√Hz)	350	1.8	124	60
Flicker Current (1Hz) (fA/√Hz)	25000	-	400	200
Corner frequency (Hz)	30	-	40	30
Bandwidth (MHz)	25	40	12	1

noise components were used to calculate the equivalent noise RTI.

1) From the sensor:
   a) the noise voltage corresponding to the equivalent resistance of the sensor (R_s), $\mathrm{n_{rb}}$;
   b) the influence of current noise on the IA, in. The latter can have two components: broadband $\mathrm{in_{BB}}$ and flicker in_f. This noise source is transformed to voltage when multiplied by the R_s of the sensor.
2) From the instrumentation amplifiers:
   a) broadband noise voltage, $\mathrm{en_{BB}}$;
   b) flicker noise voltage, en_f.

Once the sources have been identified and the operational bandwidth has been defined, the total equivalent noise at the input is expressed by the following equation; factor 2 is the result of the sensor being balanced differentially and the two branches that contribute noise:

$$\mathrm{RTI} = \sqrt{2 \cdot \mathrm{en_{rb}^2} + 2 \cdot (\mathrm{in} \cdot R_s)^2 + \mathrm{en_{BB}^2} + \mathrm{en}_f^2}. \quad (9)$$

In experimental calculations, the equivalent RTI is obtained by measuring the noise voltage at the output and by dividing it by the gain.

Table IV shows the noise source equivalent to the input RTI in real rms values for each resistance tested.

From Fig. 9, we can compare the results of the theoretical noise analysis [Fig. 9(a) based on the data in Table IV] with the data obtained in the tests [Fig. 9(b) based on the test data shown in Table V]. There is clearly a close correlation between the calculated and measured values with the greatest fidelity provided by amplifier AD524.

Using the data obtained in the tests, we also calculated the input noise spectral density, displayed in Fig. 10. An analysis of these graphs allows the following conclusions to be drawn.

1) Amplifier AD524 is the most suitable for signal sources with a low-internal impedance of approximately 1 kΩ.
2) For high values of up to 100 kΩ, amplifiers INA110 and LT1167 give similar values.
3) For values above 100 kΩ, the INA110 amplifier is ideal, providing an inappreciable current noise source compared with the other amplifiers and an absence of flicker noise.

IV. NOISE FLOOR ESTIMATE

To determine the S/N ratio in the experimental phase of real measurements using the sensor, it is necessary to determine the system noise floor as the sum of the thermal noise of the sensor, the total amplifier noise, and the A/D converter noise. A more direct procedure is to isolate the sensor away from any external noise (in an anechoic chamber) and take measurements under the same conditions as the ambient radio signal (gain, averaging time, calibration, and so on). This method requires the availability of a chamber in the ELF range that must be large enough not to affect the sensor's features, which is a situation beyond our control. Another indirect method is to take measurements, substituting the sensor by resistances whose values match the real part of Z for the sensor at various frequencies within the range of measurement.

TABLE V
RMS NOISE MEASURED (nV) AT THE INPUT RTI

	Short	1.2 kΩ	25 kΩ	110 kΩ	220 kΩ	470 kΩ
AD524	87.1	126.4	649.7	1996.4	3460.6	7302.2
INA110	177.3	201.9	474.1	933.2	1290.5	1830.9
INA126	406.3	416.3	573.9	940.7	1272.0	1806.0
LT1167	137.4	162.8	411.7	926.2	1453.1	2352.0

A. Analysis of the Signal and Noise in a Coil

To determine the spectral distribution of the total noise at the output of the sensor, it is necessary to study the behavior of the coil. Analyzing the model of Fig. 1(a), the output voltage of the coil is defined by the following:

$$V_{\mathrm{ab}} = V_s \frac{1 - \omega^2 LC_L - j\omega C_L R_L}{(1 - \omega^2 LC_L)^2 + (\omega C_L R_L)^2}. \quad (10)$$

On the other hand, the real part of the impedance presented by the coil meets

$$\mathrm{Re}(Z_{\mathrm{ab}}) = \frac{R_L}{(1 - \omega^2 LC_L)^2 + (\omega C_L R_L)^2}. \quad (11)$$

Considering that $Z_{\mathrm{ab}}(\omega)$ of the sensor coil can be measured by the VNA and known data, V_{ab} can be expressed as a function of Z_{ab}

$$V_{\mathrm{ab}} = V_S \mathrm{Re}(Z_{\mathrm{ab}}) \frac{1 - \omega^2 LC_L - j\omega C_L R_L}{R_L}. \quad (12)$$

In this particular case for setting the frequency of the sensor, the coil autoresonance is $\omega = \omega_0 = 1/(LC_L)^{1/2}$

$$V_{\mathrm{ab}}(\omega_0) = -jV_S \cdot \mathrm{Re}(Z_{\mathrm{ab}}) \sqrt{\frac{C_L}{L}} \quad (13)$$

which shows that the induced voltage in a sensing coil is directly proportional with the real part of the sensor's impedance Z_{ab}. It also shows that the maximum of the voltage induced in the sensing coil occurs in the autoresonance frequency, which corresponds well with the maximum value of the real part of the impedance of the coil. In the case of sensor 3, the maximum is placed at 55 Hz, as shown in Fig. 2. Because noise is a signal that is induced in the coil, the spectral distribution of the voltage noise corresponds to that expressed

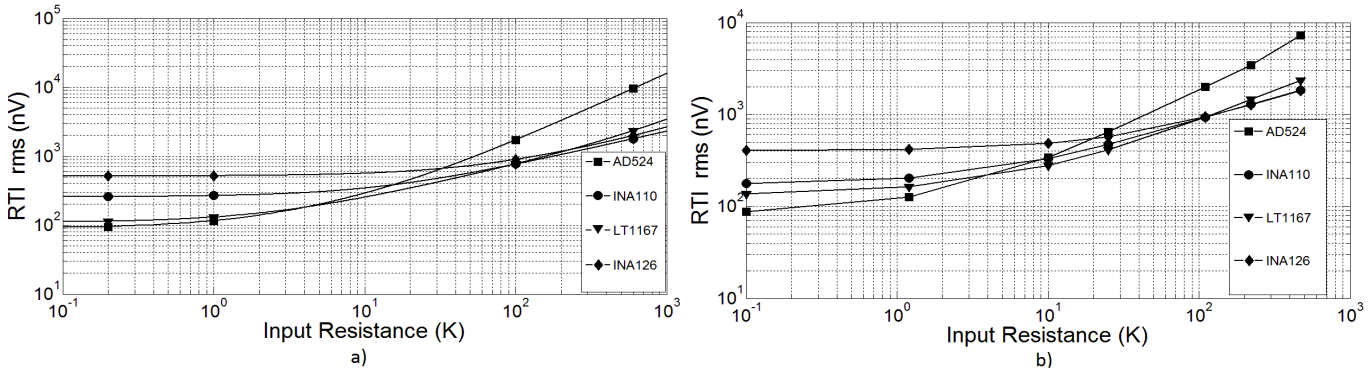

Fig. 9. Noise comparison of the four IAs. (a) Theoretical. (b) Experimental.

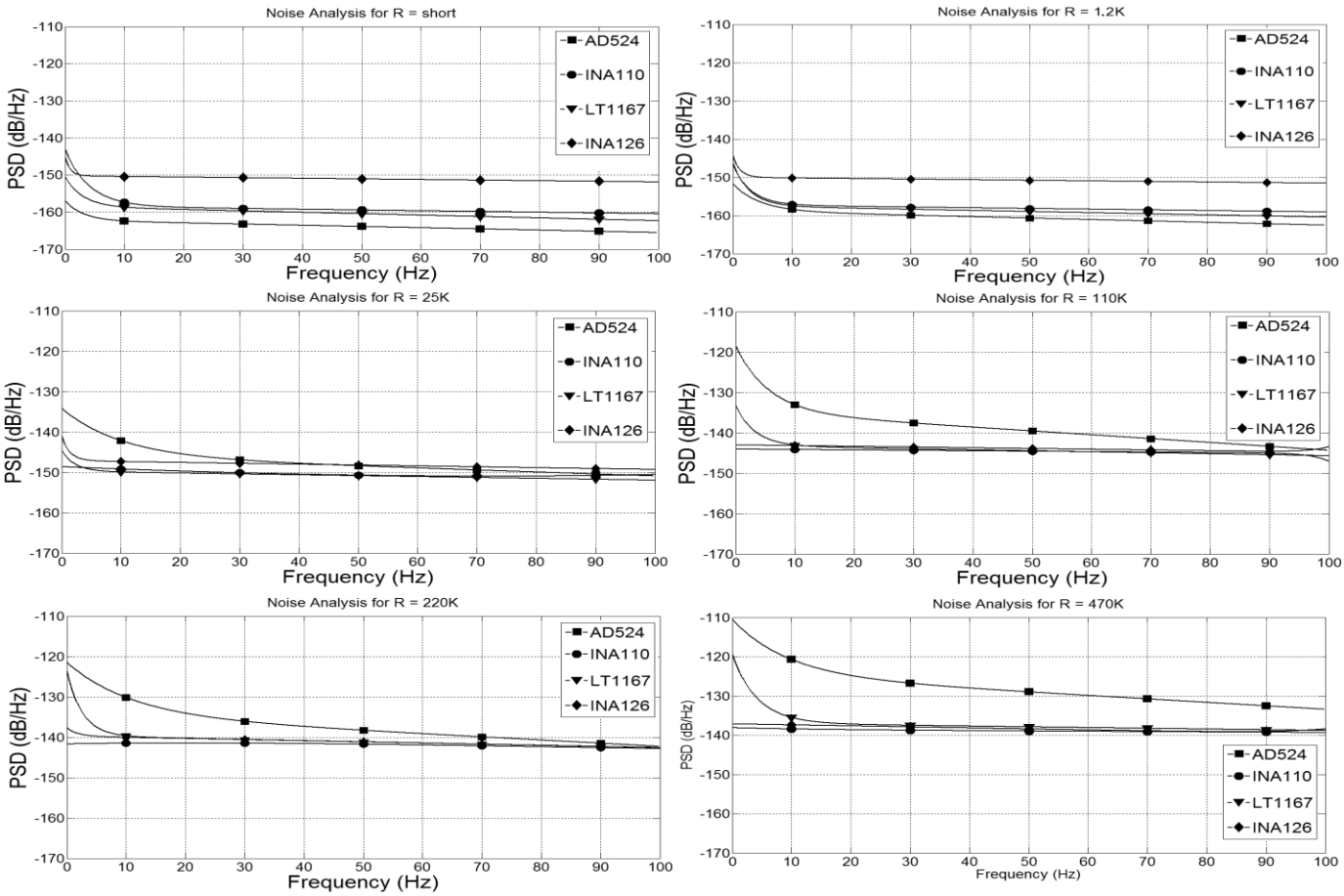

Fig. 10. Noise spectral density for different internal resistances at the source.

in (12), and the maximum of the noise spectral distribution, which is present at the autoresonance frequency of the coil sensor, is stated in (13).

B. Calculation of the Noise Floor

The indirect method is to take measurements, substituting the sensor by resistances whose values match the real part of Z for the sensor at various frequencies within the range of measurement. Using this method, we obtain the real value of the noise floor valid at frequencies corresponding to each resistor. For sensor 3, if one of the resistances selected corresponds to the maximum $\mathrm{Re}(Z)$, (in this case at 55 Hz and also for upper frequencies), the dominant noise is the noise from the sensor because the impedance of the noise floor Z_{ab} is higher than 1.5 MΩ (as shown in Fig. 2), and the noise voltage, in this case is indicated by the following equation, where k is a constant depending on the system of amplification:

$$V_n = k\sqrt{\mathrm{Re}(Z_{\mathrm{ab}})}. \tag{14}$$

This adjustment is not valid close to the origin ($f = 0$), where the influence of the noise amplifier exceeds the noise from the sensor, given that $\mathrm{Re}(Z_{\mathrm{ab}})$ is substantially lower. In this case, the previous curve is adjusted, forcing it to

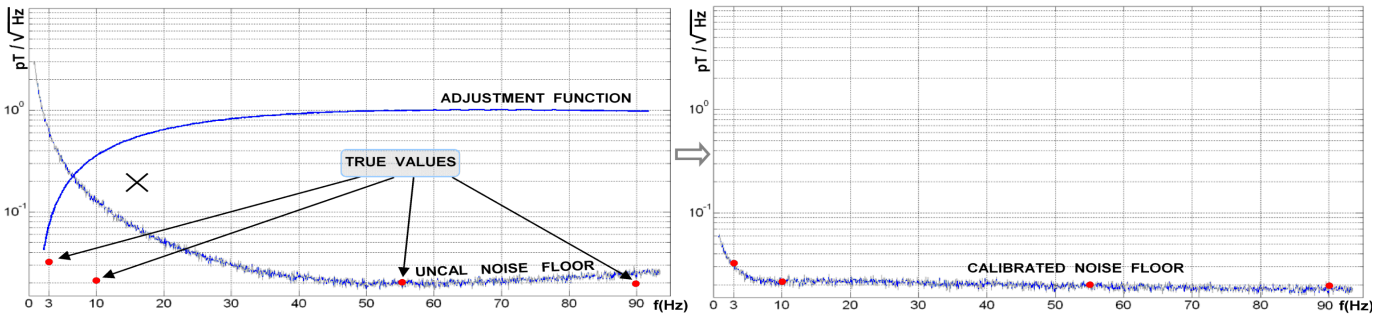

Fig. 11. Calibration process of the noise floor.

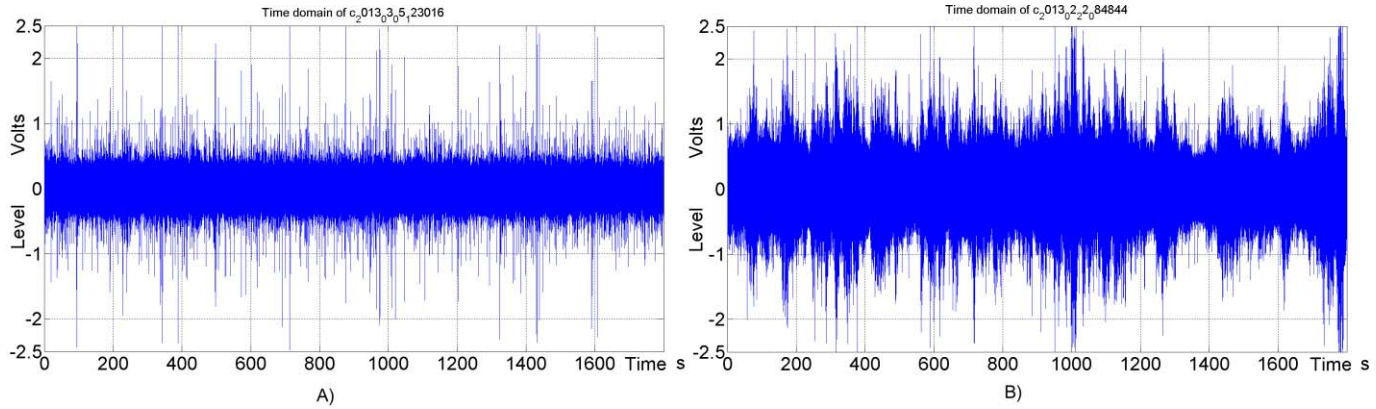

Fig. 12. Time domain signal. (A) Capture with adequate gain. (B) Capture with excessive gain.

TABLE VI
NOISE FLOOR CALIBRATION FOR THE FOUR AMPLIFIERS FOR DIFFERENT RESISTANCES

Frequency	Re[Z(f)]	AD524 (pT)	INA110 (pT)	LT1167 (pT)	INA126 (pT)
90 Hz	1.5 MΩ	$1.7\cdot10^{-1}$	$1.5\cdot10^{-2}$	$2.9\cdot10^{-2}$	$2.1\cdot10^{-2}$
55 Hz	3.3 MΩ	$1.5\cdot10^{-1}$	$1.5\cdot10^{-2}$	$2.8\cdot10^{-2}$	$2.0\cdot10^{-2}$
10 Hz	220 kΩ	$1.5\cdot10^{-1}$	$1.8\cdot10^{-2}$	$3.5\cdot10^{-2}$	$2.1\cdot10^{-2}$
3 Hz	50 kΩ	$2.0\cdot10^{-1}$	$3.0\cdot10^{-2}$	$3.8\cdot10^{-2}$	$3.4\cdot10^{-2}$

pass through various known correspondence points (Re$[Z(f)]$ at 3 Hz, Re$[Z(f)]$ at 10 Hz).

Table VI shows the level of the noise floor measured experimentally (only for sensor 3), connecting resistances to the input of the amplifiers. These resistances correspond to the ones seen by the amplifier at different frequencies, as if sensor 3 had been connected to the input.

The product of the measured noise signal, replacing the sensor by a resistor of equal value to the R_{ab}, and *adjustment function* corrects the uncalibrated signal noise outside resonance and obtains the calibrated noise floor. Fig. 11 shows the calibration process of the noise floor. The adjustment function is used as an exponential function whose coefficients depend on the true value noise points (red in Fig. 11).

The adjustment function model proposed and used in this application is implemented by setting exponential functions. The A, B, and C coefficients modify the amplitude, and the F_{C1}, F_{C2}, and F_{C3} coefficients define the frequency to apply

$$F_{\text{adjust}} = \left[1 + (A-1)e^{\frac{-f}{kF_{C1}}}\right] \cdot \left[1 + (B-1)e^{\frac{-f}{kF_{C2}}}\right] \times \left[1 + (C-1)e^{\frac{-f}{kF_{C3}}}\right]. \quad (15)$$

Equation (15) shows the adjustment function model. The amplitude coefficients A, B, and C, and the position coefficients F_{C1}, F_{C2}, and F_{C3} are calculated, so that the uncalibrated function matches in true value points. The constant k is chosen to correct a slope of exponential change. In this case, we assign the value $k = 7$.

V. RESULTS

Over the course of more than two years of operating the measurement system away from human activity, we have obtained a wealth of information. This information, properly processed, has been very useful in establishing objective criteria regarding the techniques for measuring Schumann resonances. Trials were performed using four different instruments on the first-stage amplification but ultimately used the same amplifier to be able to make a comparative study. The measurements were taken using sensor 3, comprising 300 000 turns of wire that was 0.15 mm in diameter and grouped into four windings with a 2-m-long core. The total gain was maintained at 66 dB and was adjusted to optimize the quality of the capture, achieving maximum amplification with minimal clipping. Fig. 12 shows the signal aspects in the time domain, sampled with a 24-bit A/D converter and a dynamic range of +/−2.5 V. Fig. 12(A) shows a correct

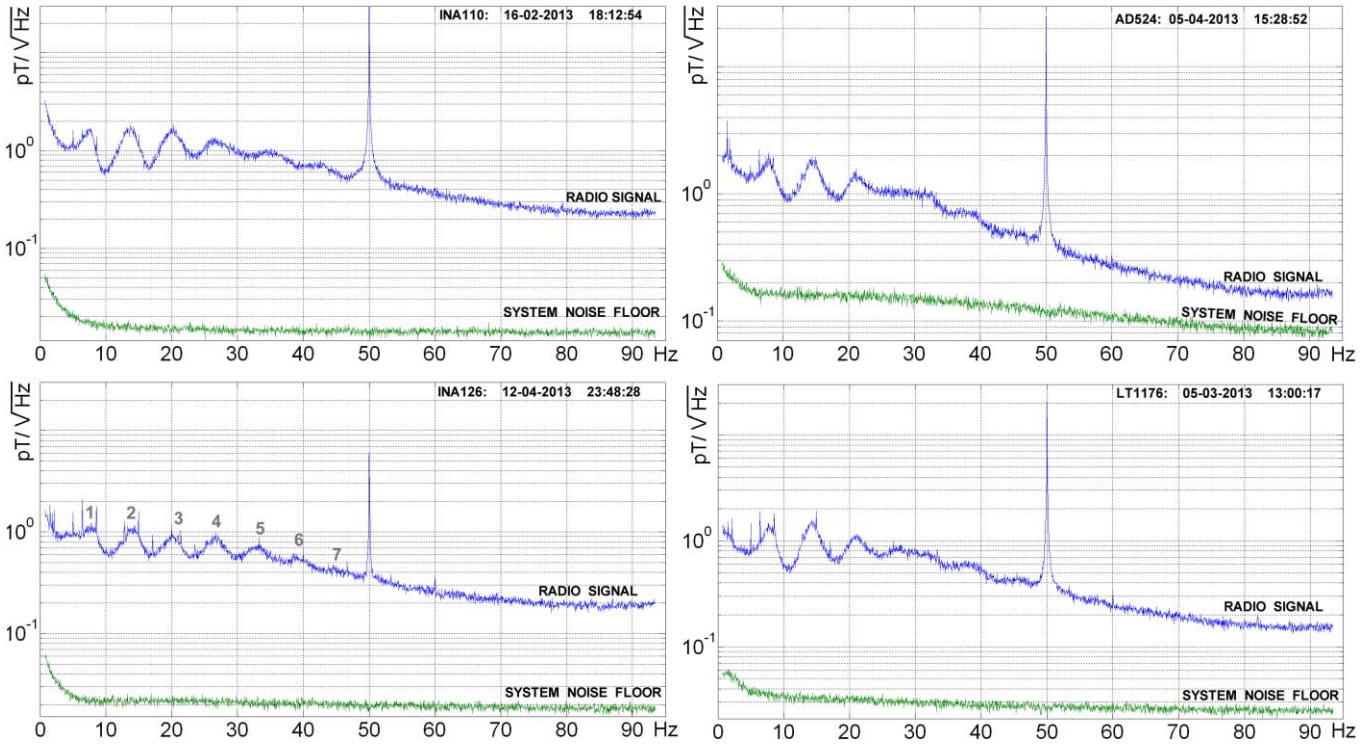

Fig. 13. Spectral averaging and system noise floor in the four amplifiers for 30 min captures.

adjustment of the gain, fixed at 66 dB ($G_{A.I.} + G_{AEND}$), while Fig. 12(B) indicates excessive gain, which results in false spectra in the frequency domain, due to the clipping effect.

The selection of four measurements was made over 30 min, each using a different IA in the frequency domain, as shown in Fig. 13. Each graph shows both the ambient radio signal and the system noise floor of the measurement. To obtain the record of the system noise floor, the sensor was substituted by the main electric supply, whose real part of the impedance coincides with that of the sensor in the frequency range 0–100 Hz, when it is isolated to avoid the capture of external fields. All of the captures were subject to the same spectral averaging procedure using temporal windows, which is the norm when studying Schumann resonances. The measurements were chosen to have a similar level of ambient signal for each amplifier to achieve objective comparisons. As shown in Fig. 13, the noise level of the system (including the noise of the sensor itself) is well below the signal level detected by the sensor for every case, even with the low-cost amplifier INA126. This indicates that any commercial IA is suitable for this purpose.

In the graphs in Fig. 13, we can see the first three modes with their greater amplitude, coincide with the references consulted. The remaining resonances are generally much more subdued, and the bandwidth is 100 Hz.

As a means of comparison, we can use the difference between the level of the mode of the first resonance and the level of the system noise floor at the same frequency (≈7.5 Hz). In this case, we obtain the following data: with the AD524, 20 dB and with the INA110, 39 dB; using the LT1167 and INA126, 31 dB. A very important factor for these results is the sensitivity of the sensor. In cases using smaller sensors with less sensitivity, the system noise floor cannot be overcome at some frequencies. The lowest frequencies are the most susceptible to this because of flicker noise. The amplifiers with lower current noise perform better in this application.

VI. Conclusion

Published state-of-the-art studies for measuring Schumann resonances reflect the interests of the researchers but do not consider improvements to the systems of measurement. Optimization of this system allows better records and shorter averaging times. We propose an optimized system of amplification for bettering the S/N ratio, and consequently the averaging time. The first stage of this system is an IA with a balanced input for the sensor and cable. We conducted a comparative study of four devices that are available from three brand leaders. Analyzing the results of more than one year of measurements, we can draw the following conclusions.

1) The type of IA is not a critical factor for the correct measurement of Schumann resonances so long as the sensor supplies a sufficient level of ambient radio signal, and the IA linearity is sufficient to avoid artifacts in the true spectra at higher frequencies. The offset does not affect this application, and the Common-Mode Rejection Ratio is not of great significance. Low-cost (3$) devices are sufficient.
2) An IA that optimizes noise in the current regime is more suitable for sensors with a large number of windings

of thin wire and exhibits high values for the real part of the impedance. Meanwhile, IAs that optimize noise in the voltage regime are better when the sensors have fewer turns, and the wire is thicker.

3) The averaging time must be as short as possible because we detected significant variations in the results of captures separated by 30 min.
4) It is very important to precisely tune the level of amplification for all stages. Determining the optimal setting may require several days of records. Using compression systems (such as A Law) to place more weight on the weak signals without clipping the strong signals does not yield good results because deviation from linearity means that restoration without an artifact is impossible.
5) The digitization stage must have the highest resolution possible: 24 bits is sufficient to allow weak signals to be recorded with adequate converter-account because the Schumann resonances have a relatively low amplitude compared with the natural ambient radio noise level. Furthermore, there must be a sufficient dynamic range to avoid clipping in accordance with the previous conclusion. The signal of interest occupies approximately 1/5 of the dynamic range.
6) The method of estimation of the noise floor, without a free signal sensor connected, yielded experimental results that provide validation and allows measurements of Schumann resonances with assured quality with captures of only 30 min, as shown in Fig. 13.

It should be noted that the results obtained with the IAs are pertinent to this particular application. For other applications with a broader bandwidth or lower input impedance (audio, PT100, and so on), the results would be different.

The solutions adopted are highly satisfactory: in the Calar Alto ELF observatory, we were able to measure the first seven resonance modes (the eighth coincides with the 50-Hz electrical power lines) with acquisition times of 15–30 min and with an S/N ratio in the fundamental mode of 39 dB, as evident in Fig. 13.

REFERENCES

[1] W. O. Schumann, "Über die strahlungslosen Eigenschwingungen einer leitenden Kugel, die von einer Luftschicht und einer onosphärenhülle umgeben ist," *Z. Naturfoschaftung Teil A*, vol. 7(2), pp. 149–154, 1952. Doi:10.1515/zna-1952-0202.

[2] Z. Nieckarz, A. Kułak, S. Zięba, M. Kubicki, S. Michnowski, and P. Barański, "Comparison of global storm activity rate calculated from Schumann resonance background components to electric field intensity E_{0Z}," *Atmos. Res.*, vol. 91, nos. 2–4, pp. 184–187, Feb. 2009.

[3] A. P. Nickolaenko, "ELF radio wave propagation in a locally nonuniform Earth-ionosphere cavity," *Radio Sci.*, vol. 29, no. 5, pp. 1187–1199, 1994.

[4] E. R. Williams, "The Schumann resonance: A global tropical thermometer," *Science*, vol. 256, no. 5060, pp. 1184–1187, May 1992.

[5] T. Bleier and F. Freund, "Earthquake [earthquake warning systems]," *IEEE Spectr.*, vol. 42, issue 12, pp. 22–27, 2005. DOI: 10.1109/MSPEC.2005.1549778.

[6] A. P. Nickolaenko, M. Hayakawa, and Y. Hobara, "Schumann resonance and global lightning activity," in *Proc. Int. Conf. Math. Methods Electromagn. Theory*, vol. 1. Jun. 1998, pp. 296–297.

[7] K. Sao, M. Yamashita, S. Tanashashi, H. Jindoh, and K. Ohta, "Experimental investigations of Schumann resonance frequencies," *J. Atmos. Terrestrial Phys.*, vol. 35, no. 11, pp. 2047–2053, Nov. 1973.

[8] F. Simões, M. Rycroft, N. Renno, Y. Yair, K. L. Aplin, and Y. Takahashi, "Schumann resonances as a means of investigating the electromagnetic environment in the solar system," *Space Sci. Rev.*, vol. 137, nos. 1–4, pp. 455–471, Jun. 2008.

[9] A. P. Nickolaenko, "Application of the Hurst exponent in the analysis of natural ELF electromagnetic noise," in *Proc. 8th Int. Conf. Math. Methods Electromagn. Theory (MMET)*, vol. 1. 2000, pp. 638–640.

[10] E. I. Yatsevich, A. V. Shvets, L. M. Rabinowich, A. P. Nickolaenko, G. G. Belyaev, and A. Y. Schekotov, "Results of comparing Schumann-resonance observations with the model of a single global thunderstorm center," *Radiophys. Quantum Electron.*, vol. 48, no. 4, pp. 254–267, Apr. 2005.

[11] Y. Tulanay *et al.*, "A case study on the ELF characterization of the Earth–ionosphere cavity: Forecasting the Schumann resonance intensities," *J. Atmos. Solar-Terrestrial Phys.*, vol. 70, nos. 2–4, pp. 669–674, Feb. 2008.

[12] V. G. Bezrodny, "Magnetic polarization of the Schumann resonances: An asymptotic theory," *J. Atmos. Solar-Terrestrial Phys.*, vol. 69, no. 9, pp. 995–1008, Jul. 2007.

[13] A. P. Nickolaenko, "Intensity of Schumann Resonance: Universal Time and Local Time Variations," Physics and Engineering of Microwaves, Millimeter and Submillimeter Waves and Workshop on Terahertz Technologies. MSMW '07. The Sixth International Kharkov Symposium on Vol: 2 pp 757–759, 2007, DOI: 10.1109/MSMW.2007.4294804.

[14] J. Rai, R. Chand, M. Israil, and S. Kamakshi, "Studies on the Schumann resonance frequency variations," in *Proc. 3rd Eur. Conf. Antennas Propag. (EUCAP)*, Mar. 2009, pp. 1437–1440.

[15] C. Bing-Xia and Q. Xiao-Lin, "Observations on Schumann resonance in low ionosphere," *J. Electron. Inf. Technol.*, vol. 32, no. 8, pp. 2002–2005, 2010.

[16] M. Füllekrug, "Detection of thirteen resonances of radio waves from particularly intense lightning discharges," *Geophys. Res. Lett.*, vol. 32, no. 13, p. 1–4, d.o.i.: 10.1029/2005GL023028 2005.

[17] A. Kruger. *Construction and Deployment of an ULF Receiver for the Study of Schumann Resonance in Iowa*. [Online]. Available: http://iihr.uiowa.edu/projects/schumann/Index.html accessed date: dec 2013.

[18] F. P. Sierra, H. S. Vazquez, M. E. Andrade, B. Mendoza, and D. Rodriguez-Osorio, "Development of a Schumann-resonance station in Mexico: Preliminary measurements," *IEEE Antennas Propag. Mag.*, vol. 40, no. 3, pp. 112–119, Jun. 2014.

[19] J. K. Hwang and P. N. Markham, "Power system frequency estimation by reduction of noise using three digital filters," *IEEE Trans. Instrum. Meas.*, vol. 63, no. 2, pp. 402–409, Feb. 2014.

[20] F. A. Levinzon, "Ultra-low-noise high-input impedance amplifier for low-frequency measurement applications," *IEEE Trans. Circuits Syst. I, Reg. Papers*, vol. 55, no. 7, pp. 1815–1822, Aug. 2008.

[21] A. Roshan-Zamir and S. J. Ashtiani, "A new method for measurement of low-frequency noise of MOSFET," *IEEE Trans. Instrum. Meas.*, vol. 62, no. 11, pp. 2993–2997, Nov. 2013.

[22] E. Serrano-Finetti and R. Pallas-Areny, "Noise reduction in AC-coupled amplifiers," *IEEE Trans. Instrum. Meas.*, vol. 63, no. 7, pp. 1834–1841, Jul. 2014.

[23] R. M. G. Salvador, J. A. G. Parra, and N. N. Castellano, "Characterization and modeling of high-value inductors in ELF band using a vector network analyzer," *IEEE Trans. Instrum. Meas.*, vol. 62, no. 2, pp. 415–423, Feb. 2013.

[24] J. G. Proakis and D. G. Manolakis, *Tratamiento Digital de Señales*, 3rd ed. Englewood Cliffs, NJ, USA: Prentice-Hall, 1998.

[25] *Impedance Measurement Function E5061B-005*, Agilent Technologies, Santa Clara, CA, USA, Dec. 2010.

[26] B. Whitlock, "Balanced lines in audio systems: Fact, fiction, and transformers," *J. Audio Eng. Soc.*, vol. 43, no. 6, pp. 454–464, Jun. 1995.

[27] A. M. Soliman, "New active RC configuration for realising a medium-selectivity notch filter," *Electron. Lett.*, vol. 8, no. 21, pp. 522–524, Oct. 1972.

[28] Analog Devices. *AD524 Datasheet*. [Online]. Available: http://www.analog.com/static/imported-files/data_sheets/AD524.pdf

[29] Texas Instruments. *INA 110 Datasheet*. [Online]. Available: http://www.ti.com/lit/ds/symlink/ina110.pdf

[30] Texas Instruments. *INA 126 Datasheet*. [Online]. Available: http://www.ti.com/lit/ds/symlink/ina126.pdf

[31] Linear Technologies. *LT1167 Datasheet*. [Online]. Available: http://cds.linear.com/docs/en/datasheet/1167fc.pdf

[32] A. Kay, *Operational Amplifier Noise: Techniques and Tips for Analyzing and Reducing Noise*, 1st ed. Amsterdam, The Netherlands: Elsevier, 2012.